THE JOURNAL OF PHYSICAL CHEMISTRY C

Article

pubs.acs.org/JPCC

Ultrasensitive Phototransistor Based on K-Enriched MoO_3 Single Nanowires

Junpeng Lu,[†,§] Cheng Sun,[‡,§] Minrui Zheng,[†] Yinghui Wang,[†] Mathews Nripan,[‡] Jeroen A. van Kan,[†] Subodh G. Mhaisalkar,*[,‡] and Chorng Haur Sow*[,†]

[†]Department of Physics, 2 Science Drive 3, National University of Singapore (NUS), 117542 Singapore

[‡]School of Materials Science and Engineering, Nanyang Technological University, Blk N4.1, Nanyang Avenue, 639798 Singapore

Supporting Information

ABSTRACT: An ultrasensitive phototransistor was fabricated based on K-intercalated MoO_3 single nanowire. Devices with ultrafast photoresponse rate, high responsivity, and broad spectral response range were demonstrated. Detailed analysis of the charge transport in the device revealed the coexistence of both thermal-activation and photoactivation mechanisms. The promising results are expected to promote the potential of this material in nano/micro-scaled photoelectronic applications.

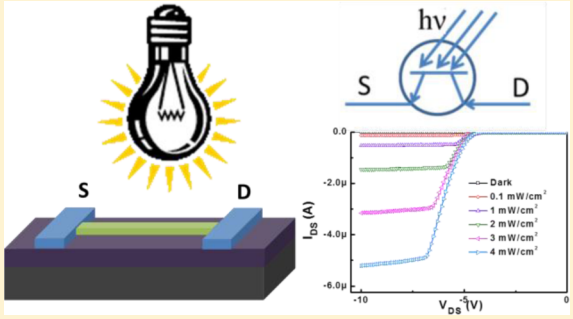

1. INTRODUCTION

Photoconductivity is one of the most studied phenomena in nanowires (NWs) mainly due to their large surface to volume ratio, nano-sized spatial constraints, and quantum confinement. They facilitate the applications of the NWs as photodetectors,[1,2] photovoltaics,[3−5] optical switches,[6] and optical interconnects. Among these, phototransistors are one of the basic building blocks for nanoelectronic circuits. Ever since the concept of the phototransistor was first proposed by William Shockley, great attention has been given to such device due to its much higher sensitivity and lower noise than those of other counterparts.[7,8] However, previously reported phototransistors either could not achieve saturated output current[9,10] or the working voltage required is excessively high (>10 V) to achieve the saturation.[11−13] Furthermore, the relatively slow response rate (ca. 100 Hz) is also an issue restraining the performance of photoelectric devices.[9,14−16] On the other hand, metal oxide nanowires form an extremely important class of photoconductors. Molybdenum oxide (MoO_3), a wide-band-gap (3.2 eV) n-type semiconductor, has attracted great attention as field emission devices (FED),[17,18] photodetectors, batteries,[19,20] catalysts,[21] sensors,[22,23] and photochromic and electrochromic materials.[24,25] Like other metal oxide nanowires, the main applications of MoO_3 in photoelectronics are limited by its wide bandgap. Its low electrical n-type conductivity (resistivity $\approx 10^{10}$ Ω·m) always inhibits its practical implementation as well.[26] Impurity doping is one of the most common approach to modify the electrical properties of the material and one advantage about MoO_3 is its rich intercalation chemistry made possible by its layered structure. However, due to the size limitation of the gap between layers, only small ions such as lithium have been successfully intercalated through immersing MoO_3 nanostructure in LiCl solution.[27] Recently, we reported the feasibility in intercalating large ions such as potassium without damaging the integrity of the layered structure of MoO_3.[28] We report here that with the intercalation of the foreign atoms the electron donor levels become extremely shallow, resulting in an ultrasensitive phototransistive process yielding a sub-millisecond level photocurrent response along with an extended response spectral range. Furthermore, saturation for the light intensity gated output current was achievable within 1 V which makes the device a promising phototransistor. We analyzed the charge transport in both negative and positive directions under different temperatures and found that charge transport may be separated into a unidirectional, thermal activated part together with a photosensitive part. This work demonstrates the potential of K-enriched MoO_3 nanowires in nano/micro-scaled photoelectric applications.

2. EXPERIMENTAL SECTION

Nanowire Synthesis. The synthesis of K-intercalated MoO_3 nanowire employed a simple and facile one-step vapor deposition method. Briefly, a piece of molybdenum foil was cleaned and loaded into the center of a horizontal tube furnace. A muscovite mica sheet ($K(Al_2)(Si_3Al)O_{10}(OH)_2$) was placed on top of the molybdenum foil with a gap of ca. 1 mm. The mica sheet not only acted as the substrate, it also provided the source of potassium. The system was ramped to 600 °C and dwelled for 6 h with controlled air flow into the chamber. Mo

Received: May 29, 2012
Revised: August 8, 2012
Published: September 24, 2012

   dx.doi.org/10.1021/jp305231j | J. Phys. Chem. C 2012, 116, 22015−22020

was evaporated from the surface of the foil and oxidized in air flow. At the surface of the substrate, the oxidized Mo vapor reacted with potassium squeezed out from the edges and grain boundaries found on the mica and then intercalated into the growing MoO_3 nanowire simultaneously to form the quasi-one-dimensional nanostructure.

Devise Fabrication. A single K_xMoO_3 nanowire was transferred to a silicon substrate coated with a 200 nm thick Si_3N_4 dielectric for device fabrication and subsequent electrical characterization. A UV-laser lithography system (Heidelberg Instruments μPG101) was employed to develop the device architecture. The fabrication was completed by thermal evaporating aluminum as the source-drain electrodes.

3. RESULTS AND DISCUSSION

After synthesis, the nanowire was transferred to a piece of silicon and the morphology of the product was identified by scanning electron microscopy (SEM). A typical SEM image of a single nanowire is shown in Figure 1a. The nanowire displays a needle-like shape with the diameter reducing slightly along the growth direction from the bottom (upper left of Figure 1a) to the top (lower right of Figuer 1a); the measured average diameter is about 800 nm with lengths in excess of 200 μm. Energy-dispersive spectroscopy (EDX) was carried out on selected spots of the nanowire, and the representative spectrum is as shown in the inset of Figure 1a. The potassium peaks are clearly demonstrated, which indicates that K atoms have been intercalated into MoO_3 successfully. We denote the K-intercalated MoO_3 nanowire as K_xMoO_3. The ratio of K/Mo revealed by the EDX spectrum is 23:77. A diode laser (emission wavelength centered at 532 nm) was employed as the excitation source for the micro-Raman (Renishaw inVia) characterization. The Raman spectra of pure MoO_3 (black line) and K_xMoO_3 nanowire (red line) are shown in Figure 1b. Evidently, the Raman shift of these two spectra are completely different,

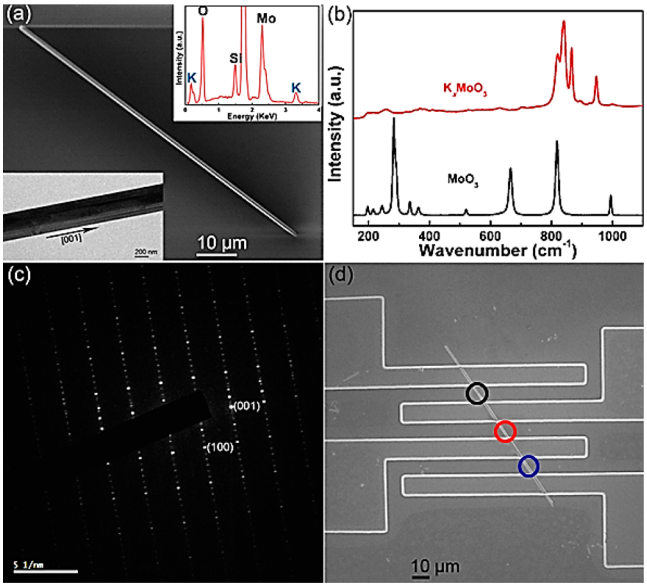

Figure 1. (a) SEM image of an individual nanowire. Upper right inset shows the EDX spectrum of the nanowire and bottom left inset shows the low-magnification TEM image. (b) Raman spectra of K-intercalated MoO_3 nanowire (red curve) and pure MoO_3 nanobelt (black curve). (c) SAED pattern of K_xMoO_3 on the (010) surface. (d) SEM image of the individual nanowire device.

which demonstrates the modification of the chemical bonds and lattice vabrations by potassium intercalation.[28] These characterization results are highly suggestive of a diversification in electrical properties of K_xMoO_3 compared with pure MoO_3. Transmission electron microscopy (TEM) was carried out to further investigate the crystalline lattice. Inset of Figure 1a illustrates the low-magnification TEM image of a single wire, and the corresponding selected area electron diffraction (SAED) pattern of K_xMoO_3 on the (010) surface is displayed in Figure 1c. Amazingly, a complicated but clear diffraction pattern was exhibited. A typical rectangular pattern consisting of large bright spots is clearly shown with five weaker spots evenly distributed between two bright spots along one direction. Through calculation, the bright spots indicate an orthorhombic configuration with the calculated lattice constants of a = 0.37 nm and c = 0.40 nm. The [001] direction is considered as the growth direction of K_xMoO_3 nanowire. The values are similar with our previously reported data of pure MoO_3 nanobelts,[29] except that a value shrinks by about 0.02 nm while c expands by about 0.03 nm compared with the K_xMoO_3 nanowire, which is attributed to the intercalation of potassium along [100] direction. Considering the valence of potassium and molybdenum, six K^+ ions exchanging with one Mo^{6+} ion from mica to nanowires can sustain the right chemical stoichiometry, which gives rise to the observed superstructure. The origin of the superstructure was detailed in our earlier report.[28]

The SEM image of an individual nanowire device with four electrodes is shown in Figure 1d. Both the electrode width and the separation between two electrodes are designed to be 10 μm. The typical $I_{DS}-V_{DS}$ curve is displayed in Figure 2a, with V_{DS} ramping from −10 to 10 V. The blue curve indicates the dark current which was carried out without any light illumination. Different from common semiconductors, the output current of K_xMoO_3 nanowire exhibited an obvious unidirectional property. The current was minimal with the rising reverse bias while at forward bias, output current increased dramatically with the voltage and almost a linear relationship was shown in the high voltage region. This curve is a typical $I-V$ characteristic curve of a diode. The equivalent circuit is diagrammed in the top inset of Figure 2a, which indicates the current is only allowed to flow from positive to negative electrode. The turn-on voltage (beyond which, the output current displays a significant positive value) of K_xMoO_3 nanowire diode is measured as $V_{d(on)}$ = 0.4 V, which is even lower than that of silicon diode ($V_{d(on)}$ = 0.5−0.6 V). The unidirectional output characteristic is attributed to the intrinsic barrier in the nanowire device. Further investigation through systematical EDX spectra along the K_xMoO_3 nanowire growth direction was carried out. And as labeled in Figure 1d, three representative spots were selected and the corresponding EDX results are shown in Figure 2b. Evidently, from bottom to top spot along the wire growth direction, the potassium concentration decreases gradually (from Mo:K = 75:25 to Mo:K = 81:19). Therefore, the formation of intrinsic barrier is attributed to the nonuniform distribution of K composition which favors the unidirectional fluxion of the electrons and inhibits the reverse channel. This property demonstrates the great potential of K_xMoO_3 nanowire as an intrinsic barrier diode for nanoscale electronics application.

Besides the diode property, K_xMoO_3 nanowire also exhibits high sensitivity to light, even under weak light intensity. A halogen lamp with the main spectrum ranging from 400 to

dx.doi.org/10.1021/jp305231j | J. Phys. Chem. C 2012, 116, 22015−22020

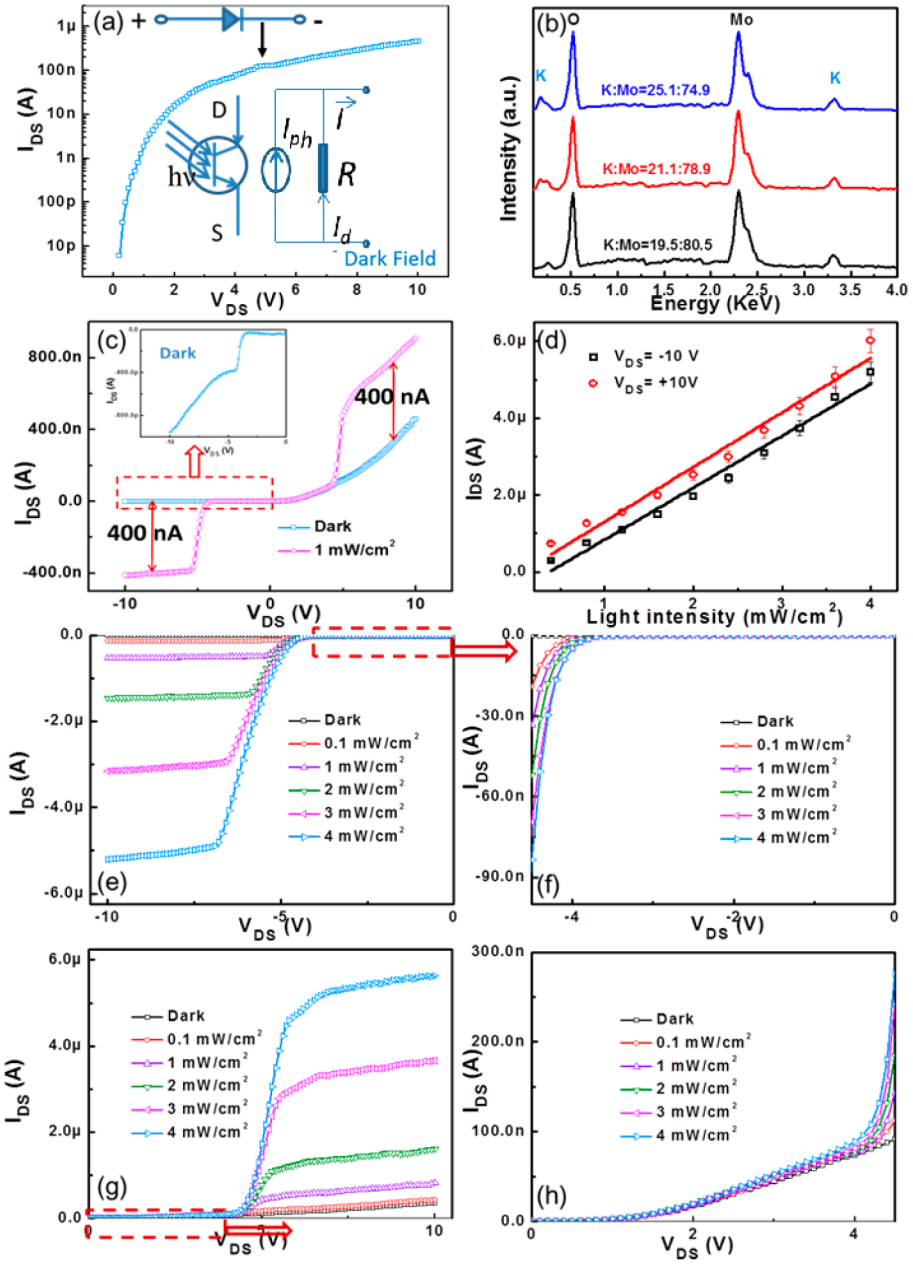

Figure 2. (a) Typical I_{DS}−V_{DS} curve of the single nanowire device in dark field. Insets show the schematic symbol of the potential applications (diode and phototransistor). (b) EDX spectra measured at three different spots along the nanowire growth direction. (c) Typical I_{DS}−V_{DS} curve (pink curve) of the single nanowire device with white light illumination. Inset zoom in the dark field curve in $V_{DS} \leq 0$ region. (d) Output current plotted as a function of light power intensity. (e) I_{DS}−V_{DS} characteristics of the device under different power illumination at the $V_{DS} \leq 0$ region. (f) Zoom in the characteristics at the region of $-4.5\ V \leq V_{DS} \leq 0$. (g) I_{DS}−V_{DS} characteristics of the device under different power illumination at the $V_{DS} \geq 0$ region. (h) Zoom in the characteristics at the region of $0 \leq V_{DS} \leq 4.5$ V.

1100 nm (the spectrum of the lamp was captured using a spectrometer and the result is shown in the Supporting Information Figure S1) was employed as white light to study the photoresponse of the nanowire device during I−V measurement. The pink curve shown in Figure 2c displays the typical I_{DS}−V_{DS} curve under 1 mW/cm^2 of broad beam white light illumination. Obviously, the output current increased sharply beyond 4 V (−4 V for backward) and subsequently reached saturation before 5 V for both voltage direction. A change in magnitude of 400 nA was registered in this case. The rapid increase and saturation of the photorelated current suggests the potential of K_xMoO_3 nanowire as a ultrasensitive phototransistor. In Figure 2d, the magnitude of the current as a function of the power intensity of white light was also recorded, in which case the voltage was kept at −10 V (black square) and 10 V (red circle). The output current increased with increasing light power intensity, and a linear relationship is noted, with larger values of the current at +10 V caused by higher dark currents in the positive voltage regime. This typical illumination characteristic curve demonstrates the good performance of K_xMoO_3 single nanowire phototransistor. Phototransistors are built on photorelated free carriers under illumination. Hence, two working mechanisms may occur in this phototransistor device. One is photovoltaic effect which depends on the light absorption, exciton dissociation, electron and hole diffusion, and electrode collections.[9] The other

dx.doi.org/10.1021/jp305231j | J. Phys. Chem. C 2012, 116, 22015−22020

possible mechanism is photoconductive effect which results in a huge increase of carrier density in the nanowire ($\sigma = nq\mu$, where σ is the conductivity, μ is the carrier mobility of the material, n is the carrier density, and q is the charge of electron). In the present system, no photovoltage was observed in the device despite the formation of a large photocurrent. Hence, the photoconductive effect is more significant and can be described by[15,30]

$$I_{pc} = (q\mu nE)WD = AP_{power} \quad (1)$$

where E is the electrical field in the nanowire, W is the gate width, and D is the active layer thickness, while P_{power} is the incident light power and A is a fitting parameter. Evidently, the experimental data in Figure 2d are well fitted with eq 1, providing further credence to the theory that the photocurrent of K_xMoO_3 single nanowire device was driven by photoconductive effect. For a fixed incident light power intensity, the density of the excited free charge carriers was fixed, and thus the magnitude of the photocurrent remained the same for applied voltages that were larger than the threshold (as shown in Figure 2c).

The output characteristics under different intensities of illumination at the negative voltage direction are shown in Figure 2e. With the increase of incident light power intensity, the drain current rose gradually. Actually, the drain current was controlled by the optical power density, and the curves displayed good transistor behavior, consisting of a rapidly increasing linear regime and a fully saturated regime, which is similar to the output characteristics of a traditional field effect transistor modified by gate voltage, except here the light intensity plays the role of voltage gating. The results suggest that the incident light could be employed to replace the gate voltage, V_{GS}, as an additional terminal to control the output level of the transistor, indicating an effective approach to achieve current modification and signal magnification in a single nanowire device for future low-cost, nanoscale photoelectric integration. Under 4mW/cm^2 illumination, the I_{DS} is measured to be -5.6 μA at $V_{DS} = -10$ V with the electric conductivity estimated to be about 3.3 S/m. The responsivity, R_{res}, an important parameter of phototransistors, can be calculated by[31]

$$R_{res} = \frac{I_{ph}}{P_{opt}} = \frac{(I_{DS,illum} - I_{DS,dark})S^{-1}}{P_{inc}} \quad (2)$$

where P_{opt} is the light power, $I_{DS,illum}$ and $I_{DS,dark}$ are the drain-source current under illumination and in dark, respectively, S is the effective area of nanowire device, and P_{inc} is power density of the incident light. It is very attractive that the R_{res} value of the nanowire phototransistor could reach as high as 1.75×10^7 mA/W under white incident light with a wavelength centered around 630 nm and a 6 V drain voltage bias. This value is much higher than that of graphene (~1 mA/W),[32] MoS_2 (7.5 mA/W),[10] and organic phototransistors (PPEs, 36 mA/W).[15] It is even comparable with those of the ZnO nanowires (1.29×10^7 mA/W)[16] and vertially aligned Si nanowire arrays (~10^8 mA/W).[33] The high responsivity of the nanowire device enables a large on/off ratio, indicating the potential applications of the nanowire transistor in photoelectronic devices such as retrosensors, optoisolators,[9,31] and photoamplifiers. The related diagram and equivalent circuit of the K_xMoO_3 nanowire transistor are illustrated in the right inset of Figure 2a, where R is the intrinsic resistance of K_xMoO_3 nanowire. The output characteristics of I_{DS} under illumination at positive V_{DS} direction is shown in Figure 2g. Similarly, the device also showed a good phototransistor behavior. The output current was well controlled by incident light power, and saturation is achieved at higher voltage regime. Again, the unidirectional property of the existing current in K_xMoO_3 nanowire resulted in the slightly higher output current compared with the negative voltage region. Careful analysis of the output characteristics could indicate more details about the phototransistor mechanism, as shown in Figure 2f,h. The regions for -4.5 V $\le V_{DS} \le 0$ and $0 \le V_{DS} \le 4.5$ V were zoomed in, and it is clear that the photo-related current is only prominent when the drain voltage is beyond 4 V (or -4 V). This is attributed to the Schottky barrier formed by the connection of K_xMoO_3 nanowire and aluminum electrode (the work function of Al is about 4.2 eV[34]). The existing output curve under dark field was further investigated. As shown in the inset of Figure 2c, which is the zoom in of the negative voltage regime of the dark characteristics, a small current was detected at around -4 V and increased with the increasing magnitude of the voltage thereafter, which indicates a typical Schottky contact characteristic curve. We should also note that there is also a small kink at +4 V for the data shown in Figure 2a (indicated by black arrow). Therefore, the whole output characteristic is attributed to be a combination of two possible mechanisms: one is the unidirectional output caused by intrinsic nonuniform potential distribution (denoted as part I), and the other is a normal semiconductor output with Schottky contact (part II), as shown in Figure 3. Since the magnitude of the output current

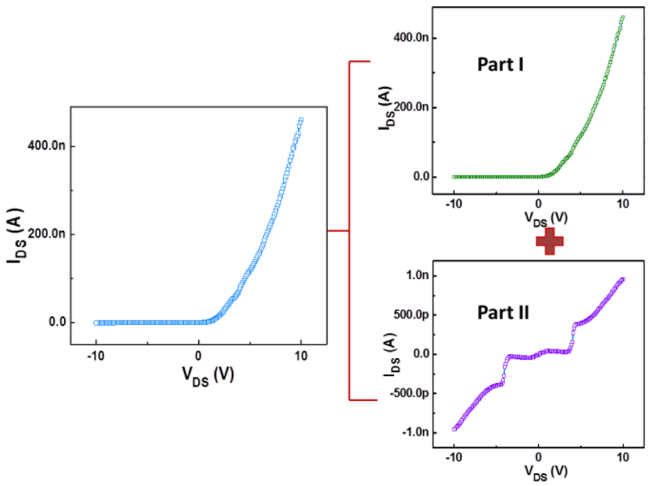

Figure 3. Illustration of the proposal that the entire output characteristic of the device comprises of unidirectional output caused by intrinsic nonuniform potential distribution within the nanowire (part I) and normal semiconductor output with Schottky contact (part II).

related to part I is much higher than that of part II, part I dominated the output characteristic curve in dark condition by showing the unidirectional tendency of the entire output current.

Although the output of part I showed little fluctuation with incident light power intensity, it changed dramatically with thermal variation. The output current was measured with temperature varying from 77 to 330 K, and the corresponding I_{DS} curves were recorded. As shown in Figure 4a, the V_{DS} values were kept at 2, 3, and 4 V, at which region I_{DS} is hardly affected by the incident light. An exponential behavior of the output

dx.doi.org/10.1021/jp305231j | J. Phys. Chem. C 2012, 116, 22015−22020

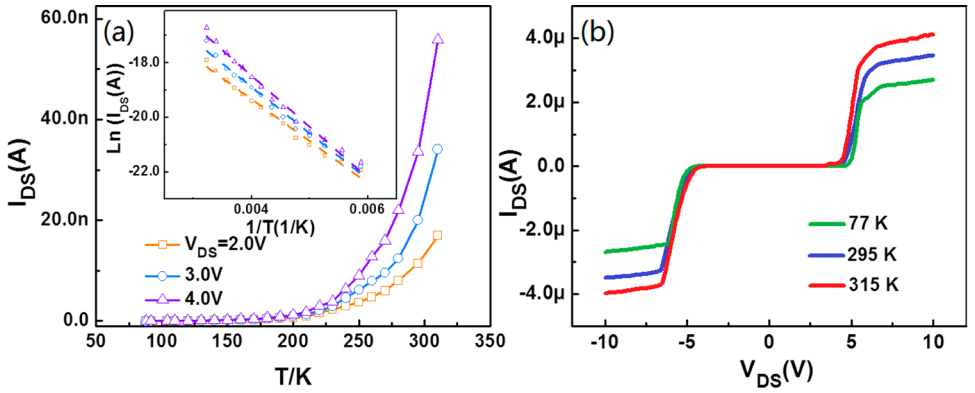

Figure 4. (a) Low-temperature dependence of the output current, V_{DS} = 2, 3, and 4 V. Inset is the relationship between ln(I_{DS}) and 1/temperature. (b) Typical I_{DS}−V_{DS} characteristics of the device at different temperatures.

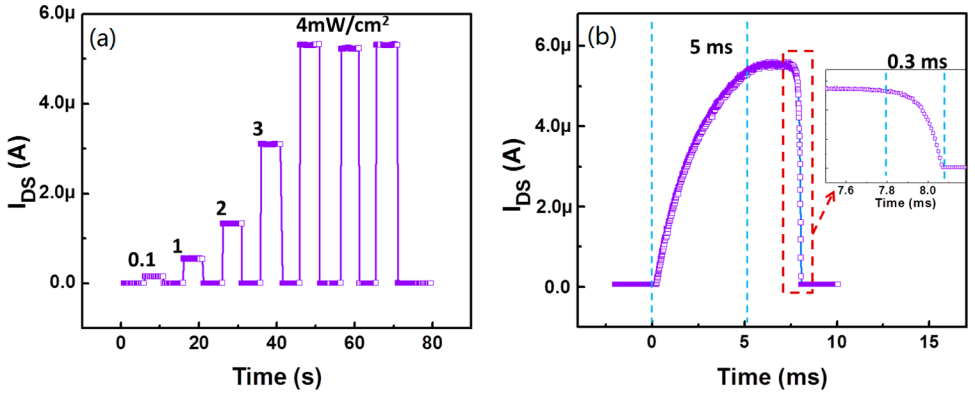

Figure 5. (a) Photoresponse characteristics of K_xMoO_3 phototransistor at different optical power. (b) Photoswitching rate test of the device.

current with increasing temperature is demonstrated for various applied bias. The electron movement almost came to a stop below 100 K and increased rapidly with rising temperature from 200 to 330 K. The corresponding values of ln(I_{DS}) display a quasi-linear relationship with the increasing temperature, as shown inset of Figure 4a. As expected, the current−temperature dependence of the nanowire follows the thermal activation model[33,35]

$$I_{DS} = \sigma_0 \frac{V_{DS} S_{cross}}{W} e^{-\Delta E/K_B T} \quad (3)$$

where W is the width of the transistor channel, S_{cross} is the cross-sectional area of the K_xMoO_3 nanowire, k_B is the Boltzmann constant, and ΔE is activation energy. The fitted results of the phototransistor at various applied bias were shown as solid lines in Figure 4a. The activation energy was found to be $\Delta E \sim 0.69$ eV. Evidently, all the output current at V_{DS} below 4 V region were fitted well with the thermal activation model, indicating the thermal activation characteristic of K_xMoO_3 nanowire in part I rather than optoactivation. On the other hand, Figure 4b exhibits the typical characteristic curves under 3 mW/cm^2 illumination at different temperature (where we recorded the total outputs and deducted the dark field curve). Obviously, the photocurrent also shows an obvious dependence on temperature, indicating that both photo-activated thermal-activated processes in part II (at high voltage bias) under illumination conditions. The obvious thermal- and photoactivation process demonstrated the potential of K_xMoO_3 nanowires in both thermal-electronic and photoelectronic applications dependent on different bias applied.

The promising phototransistor performance is also supported by the ultrafast photoresponse of the K_xMoO_3 nanowire to light. The time responses of the transistor have been investigated under applied bias V_{DS} = 10 V with light power densities of 0.1, 1, 2, 3, and 4 mW/cm^2. The light source was turned on and off for 5 s. As shown in Figure 5a, the device presented a rapid on/off switching behavior. Each photoresponse cycle consists of three distinct stages: a sharp rise, a steady state, and a sharp decay process to original state with an on/off current ratio of about 10^4 under 4 mW/cm^2 illumination. Five single nanowire devices have been tested and the on/off ratio ranges from 1 × 10^4 to 5.6 × 10^4. Photoresponse behavior of another device fabricated and studied is shown in the Supporting Information Figure S2. As shown in Figure 5b, both the response and recovery process were completed rapidly. The rapid response time (ca. 5 ms) was tested by an oscilloscope (DSO-X 3024A, 200 MHz) associated with an electronic chopper. As shown in the inset of Figure 5b, the recovery rate was tested to be as short as 0.3 ms, which is even faster than the rising response process, 5 ms. These values (3.3 and 0.2 kHz) are much faster than that of the reported organic (F16CuPc, 50 and 100 Hz, and TA-PPE) and inorganic (ZnO) phototransistors or photoswitches.[9,15,16] The device also exhibited high stability and reproducibility. Almost no degradation of the current was observed after several tens of cycles of continuous work, as shown in the Supporting Information Figure S3. Moreover, the phototransistor is demonstrated to respond to full spectrum regime. The photoresponse characteristics were further investigated with the help of a series of filters with wavelength selection centered

dx.doi.org/10.1021/jp305231j | J. Phys. Chem. C 2012, 116, 22015−22020

at 488, 500, 514, 532, 550, 570, 600, and 633 nm and lasers with wavelengths of 325, 532, 808, and 1064 nm. The representative results and photocurrent as a function of wavelength are shown in the Supporting Information Figures S4 and S5. Evidently, the K_xMoO_3 nanowire device is much more sensitive for the visible spectrum regime which promotes this kind of devices toward a myriad of applications in daily life.

4. CONCLUSION

In summary, we managed to synthesize the K-intercalated MoO_3 nanowire through a simple but effective one-step vapor deposition method. EDX analysis confirmed the decreasing trend of K concentration along the nanowire growth direction which enables the unidirectional, diode-like behavior of the dark current. This part of current is found to be irresponsive to the change of light intensity, but it is responsive to changes in temperature. The extreme shallow donor created by the intercalation of K enables an ultrasensitive and submillisecond photocurrent response. On top of this, fabrication and characterization of the single-wire device demonstrated that the saturation of the output current can be achieved within a voltage window of 1 V (from 4 to 5 V), and light was able to serve as a reliable control over the current level with the on/off ratio as high as 10^4, which confirms the application of the devices as promising phototransistors and light sensors. Moreover, the high responsivity and broad spectral response further illustrate the potential of this material in the nanosized, photoelectronic applications of communications, sensing, and imaging.

■ ASSOCIATED CONTENT

Ⓢ Supporting Information

Spectrum of light source, typical $I_{DS}-V_{DS}$ curve and photoresponse of another representative device, long time trace of photoresponse and photoresponse under different wavelength light. This material is available free of charge via the Internet at http://pubs.acs.org.

■ AUTHOR INFORMATION

Corresponding Author

*E-mail: subodh@ntu.edu.sg (S.G.M.); physowch@nus.edu.sg (C.H.S.).

Author Contributions

The manuscript was written through contributions of all authors. All authors have given approval to the final version of the manuscript.

Author Contributions

§These authors contributed equally.

Notes

The authors declare no competing financial interest.

■ ACKNOWLEDGMENTS

This work is supported by the Singapore National Research Foundation under CRP Award NRF-CRP-4-2008-03. The authors gratefully acknowledge the financial support.

■ REFERENCES

(1) Soci, C.; Zhang, A.; Bao, X. Y.; Kim, H.; Lo, Y.; Wang, D. L. *J. Nanosci. Nanotechnol.* **2010**, *10*, 1430−1449.
(2) Soci, C.; Zhang, A.; Xiang, B.; Dayeh, S. A.; Aplin, D. P. R.; Park, J.; Bao, X. Y.; Lo, Y. H.; Wang, D. *Nano Lett.* **2007**, *7*, 1003−1009.
(3) Hu, L.; Chen, G. *Nano Lett.* **2007**, *7*, 3249−3252.
(4) Tian, B.; Kempa, T. J.; Lieber, C. M. *Chem. Soc. Rev.* **2009**, *38*, 16−24.
(5) Huynh, W. U.; Dittmer, J. J.; Alivisatos, A. P. *Science* **2002**, *295*, 2425−2427.
(6) Kind, H.; Yan, H. Q.; Messer, B.; Law, M.; Yang, P. D. *Adv. Mater.* **2002**, *14*, 158−160.
(7) Seeds, A. J.; De Salles, A. A. A. *IEEE Trans. Microwave Theory Tech.* **1990**, *38*, 577−585.
(8) Saragi, T. P. I.; Pudzich, R.; Fuhrmann, T.; Salbeck, J. *Appl. Phys. Lett.* **2004**, *84*, 2334−2336.
(9) Tang, Q.; Li, L.; Song, Y.; Liu, Y.; Li, H.; Xu, W.; Liu, Y.; Hu, W.; Zhu, D. *Adv. Mater.* **2007**, *19*, 2624−2628.
(10) Yin, Z.; Li, H.; Li, H.; Jiang, L.; Shi, Y.; Sun, Y.; Lu, G.; Zhang, Q.; Chen, X.; Zhang, H. *ACS Nano* **2011**, *6*, 74−80.
(11) Singh, T. B.; Koeppe, R.; Sariciftci, N. S.; Morano, M.; Brabec, C. J. *Adv. Funct. Mater.* **2009**, *19*, 789−795.
(12) Guo, Y.; Du, C.; Di, C.-a.; Zheng, J.; Sun, X.; Wen, Y.; Zhang, L.; Wu, W.; Yu, G.; Liu, Y. *Appl. Phys. Lett.* **2009**, *94*, 143303−143303.
(13) Zhang, A.; You, S.; Soci, C.; Liu, Y.; Wang, D.; Lo, Y.-H. *Appl. Phys. Lett.* **2008**, *93*, 121110−121113.
(14) Varghese, B.; Tamang, R.; Tok, E. S.; Mhaisalkar, S. G.; Sow, C. H. *J. Phys. Chem. C* **2010**, *114*, 15149−15156.
(15) Dong, H.; Li, H.; Wang, E.; Nakashima, H.; Torimitsu, K.; Hu, W. *J. Phys. Chem. C* **2008**, *112*, 19690−19693.
(16) Weng, W. Y.; Chang, S. J.; Hsu, C. L.; Hsueh, T. J. *ACS Appl. Mater. Interfaces* **2011**, *3*, 162−166.
(17) Zhou, J.; Xu, N. S.; Deng, S. Z.; Chen, J.; She, J. C.; Wang, Z. L. *Adv. Mater.* **2003**, *15*, 1835−1840.
(18) Zhu, Y. W.; Yu, T.; Cheong, F. C.; Xu, X. J.; Lim, C. T.; Tan, V. B. C.; Thong, J. T. L.; Sow, C. H. *Nanotechnology* **2005**, *16*, 88.
(19) Juárez Ramírez, I.; Martínez-de la Cruz, A. *Mater. Lett.* **2003**, *57*, 1034−1039.
(20) Reddy, C. V. S.; Qi, Y. Y.; Jin, W.; Zhu, Q. Y.; Deng, Z. R.; Chen, W.; Mho, S. I. *J. Solid State Electrochem.* **2007**, *11*, 1239−1243.
(21) Ohler, N.; Bell, A. T. *J. Catal.* **2005**, *231*, 115−130.
(22) Barazzouk, S.; Tandon, R. P.; Hotchandani, S. *Sens. Actuators, B* **2006**, *119*, 691−694.
(23) Hussain, O. M.; Rao, K. S. *Mater. Chem. Phys.* **2003**, *80*, 638−646.
(24) Hsu, C.-S.; Chan, C.-C.; Huang, H.-T.; Peng, C.-H.; Hsu, W.-C. *Thin Solid Films* **2008**, *516*, 4839−4844.
(25) Mahajan, S. S.; Mujawar, S. H.; Shinde, P. S.; Inamdar, A. I.; Patil, P. S. *Appl. Surf. Sci.* **2008**, *254*, 5895−5898.
(26) Wisitsoraat, A.; Phokharatkul, D.; Tuantranont, A.; Saikaew, C. *Effect of Carbon Doping on Gas Sensing Properties of Molybdenum Oxide Nanoneedles*; IEEE: New York, 2009; pp 312−315.
(27) Mai, L. Q.; Hu, B.; Chen, W.; Qi, Y. Y.; Lao, C. S.; Yang, R. S.; Dai, Y.; Wang, Z. L. *Adv. Mater.* **2007**, *19*, 3712−3716.
(28) Hu, Z.; Zhou, C.; Zheng, M.; Lu, J.; Varghese, B.; Cheng, H.; Sow, C. H. *J. Phys. Chem. C* **2012**, *116*, 3962−3967.
(29) Xie, Y. L.; Cheong, F. C.; Zhu, Y. W.; Varghese, B.; Tamang, R.; Bettiol, A. A.; Sow, C. H. *J. Phys. Chem. C* **2009**, *114*, 120−124.
(30) Sze, S. M. *Phys. Semicond. Devices* **1988**, 744.
(31) Hamilton, M. C.; Martin, S.; Kanicki, J. *IEEE Trans. Electron Devices* **2004**, *51*, 877−885.
(32) Xia, F.; Mueller, T.; Lin, Y.-m.; Valdes-Garcia, A.; Avouris, P. *Nat. Nanotechnol.* **2009**, *4*, 839−843.
(33) Zhang, A.; Kim, H.; Cheng, J.; Lo, Y.-H. *Nano Lett.* **2010**, *10*, 2117−2120.
(34) Bennette, C. J. S.; Swanson, L. W.; Charbonnier, F. M. *J. Appl. Phys.* **1967**, *28*, 634.
(35) Ma, Y. *Solid State Commun.* **2004**, *130*, 313−316.